

Combined Analysis of Electric Dipole Moments and Lepton Flavor Violating Rare Decays ^{*}

Y. Ayazi and Y. Farzan

Institute for research in fundamental sciences (IPM), P.O. Box 19395-5531, Tehran, Iran

In the context of general Minimal Supersymmetric Standard Model (MSSM), new sources for Lepton Flavor Violation (LFV) as well as CP-violation appear. We show that in the presence of LFV sources, the electric dipole moment of the electron (d_e) can receive new contributions. In particular, d_e can receive a significant contribution at one loop level from the phase of the trilinear A -term of the staus, ϕ_{A_τ} . We discuss how we can derive information on ϕ_{A_τ} by combining the information on d_e with that on the LFV decay modes of the τ lepton. We then discuss if this approach can be considered as an alternative to the direct measurement of ϕ_{A_τ} at ILC.

1. INTRODUCTION

As is well-known, nonzero electric dipole moment of elementary particles would indicate CP-violation. In the context of SM, there is an established source of CP-violation which is the famous phase of the CKM matrix. However, the contribution of this phase to d_e is smaller than $10^{-38} e \text{ cm}$ [1] which is too small to be probed in any foreseeable future [2]. The phases in the neutrino mass matrix can also contribute to d_e but their contribution is suppressed by fourth power of neutrino mass and is quite negligible: $O(10^{-73}) e \text{ cm}$ [3]. Thus, detection of a nonzero d_e at future experiments [2] would open a window on new physics.

Another class of phenomena that can teach us about new physics are Lepton Flavor Violating (LFV) rare decays of charged leptons: *i.e.*, $\mu \rightarrow e\gamma$, $\tau \rightarrow e\gamma$ and $\tau \rightarrow \mu\gamma$. It is by now established that the violation of lepton flavor takes place in the neutrino oscillation phenomenon; however, if the source of LFV is merely the neutrino mass matrix, the rate of LFV will be extremely low [4] and below the sensitivity of any search in the foreseeable future. Thus, if the future searches record a positive signal, it will be an indication for new physics.

The scale of the new physics might lie at high energies (100 GeV or higher) but we can learn about the properties of the new physics by studying the indirect effects on low energy phenomena such as Electric Dipole Moment (EDM) and/or LFV rare decay of charged leptons. If there is a way to check what we have learned from the low energy phenomena by direct measurements at high energy labs, the results will be more exciting. The former can be considered as a guideline for the latter.

Minimal Supersymmetric Standard Model (MSSM), which is arguably the most popular extension of the SM, introduces several sources for CP-violation as well as sources for LFV which can lead to effects exceeding the present experimental bounds. The experimental bounds on $\text{Br}(\ell_j \rightarrow \ell_i \gamma)$ and the EDM of the elementary particles constrain the sources of LFV and CP-violation, respectively. In the context of MSSM with vanishing LFV sources, the bounds from the EDMs on the CP-violating phases have been extensively studied in the literature (for an incomplete list see [5, 6, 7]). Although A_τ (trilinear coupling of the staus in the soft potential) is a LF conserving coupling, in the presence of LFV, it can affect the properties of leptons of other generations. In particular, in the presence of LFV, the phase of A_τ can contribute to d_e at one loop level [8]. In [8], the bounds on the LFV elements of the trilinear A -couplings from the stability of vacuum was overlooked. In this paper, we take into account these bounds and demonstrate that at certain parts of the parameter space, these bounds reduce ambiguities in the interpretation of results and helps us to derive conclusive bounds.

^{*}Presented at ICHEP 08 by Y. Farzan as the IUPAP young scientist prize ceremony talk

2. SOURCES OF CP-VIOLATION AND LFV IN THE MSSM

The phenomenology of MSSM is determined by its superpotential and the soft supersymmetry breaking potential. The part of the superpotential relevant for this study is

$$W_{\text{MSSM}} = -Y_i \widehat{e}_{Ri}^c \widehat{L}_i \cdot \widehat{H}_d - \mu \widehat{H}_u \cdot \widehat{H}_d \quad (1)$$

where \widehat{L}_i , \widehat{H}_u and \widehat{H}_d are doublets of chiral superfields respectively associated with doublet $(\nu_i e_{Li})$ and the two Higgs doublets of the MSSM. In the above formula, \widehat{e}_{Ri}^c is the chiral superfield associated with the right-handed charged lepton field e_{Ri} . The index “ i ” determines the flavor. We have written the superpotential in the mass basis of charged leptons (*i.e.*, Yukawa coupling of the charged leptons is taken to be diagonal). At the electroweak scale, the part of the soft supersymmetry breaking potential relevant for this study can be written as

$$\begin{aligned} \mathbf{L}_{\text{soft}}^{\text{MSSM}} &= -1/2 \left(M_1 \widetilde{B}\widetilde{B} + M_2 \widetilde{W}\widetilde{W} + \text{H.c.} \right) \\ &- \left((A_i Y_i \delta_{ij} + A_{ij}) \widetilde{e}_{Ri}^c \widetilde{L}_j \cdot H_d + \text{H.c.} \right) - \widetilde{L}_i^\dagger (m_{eL}^2)_{ij} \widetilde{L}_j - \widetilde{e}_{Ri}^c{}^\dagger (m_{eR}^2)_{ij} \widetilde{e}_{Rj}^c \\ &- m_{H_u}^2 H_u^\dagger H_u - m_{H_d}^2 H_d^\dagger H_d - (B_H H_u \cdot H_d + \text{H.c.}), \end{aligned} \quad (2)$$

where the “ i ” and “ j ” indices determine the flavor and \widetilde{L}_i consists of $(\tilde{\nu}_i \tilde{e}_{Li})$. Notice that we have divided the trilinear coupling to a flavor diagonal part $(A_i Y_i \delta_{ij})$ and a LFV part $(A_{ij}$ with $A_{ii} = 0)$. Terms involving the squarks as well as the gluino mass term have to be added to Eq. (2). The Hermiticity of the Lagrangian implies that $m_{H_u}^2$, $m_{H_d}^2$ and the diagonal elements of m_{eL}^2 and m_{eR}^2 are all real. Moreover, without loss of generality we can rephase the fields to make M_2 , B_H and Y_i real. In such a basis, the rest of the above parameters can in general be complex and can be considered as sources of CP-violation giving contributions to the EDMs.

After electroweak symmetry breaking, the slepton mass terms can be written as

$$L_{\text{slepton}} = - \sum_{i,j} \begin{pmatrix} \widetilde{e}_{Li}^\dagger & \widetilde{e}_{Ri}^\dagger \end{pmatrix} \begin{pmatrix} (m_L^2)_{ij} & (m_{LR}^2)_{ij} \\ (m_{LR}^2)_{ij} & (m_R^2)_{ij} \end{pmatrix} \begin{pmatrix} \widetilde{e}_{Lj} \\ \widetilde{e}_{Rj} \end{pmatrix}, \quad (3)$$

where

$$(m_L^2)_{ij} = (m_{eL}^2)_{ij} + (m_e^2)_i \delta_{ij} + m_Z^2 \cos 2\beta \left(-\frac{1}{2} + \sin^2 \theta_W \right) \delta_{ij} \quad (4)$$

$$(m_R^2)_{ij} = (m_{eR}^2)_{ij} + (m_e^2)_i \delta_{ij} - m_Z^2 \cos 2\beta \sin^2 \theta_W \delta_{ij} \quad (5)$$

and

$$(m_{LR}^2)_{ij} = m_i (A_i - \mu^* \tan \beta) \delta_{ij} + A_{ij} \langle H_d \rangle \quad (6)$$

in which $\tan \beta = \langle H_u \rangle / \langle H_d \rangle$. The sources of LFV are $(m_L^2)_{ij}$, $(m_R^2)_{ij}$ and $(m_{LR}^2)_{ij} = A_{ij} \langle H_d \rangle$ with $i \neq j$. In the absence of LFV, at one loop level, each of A_α can contribute to the electric dipole moment of only the corresponding charged lepton e_α . For example, d_e receives a significant contribution from the phase of A_e at one loop level but if $(m_L^2)_{e\tau} = (m_R^2)_{e\tau} = A_{e\tau} = A_{\tau e} = 0$, the phase of A_τ cannot induce any contribution to d_e at one loop level. At the two loop level, imaginary A_τ can induce a contribution to d_e but the effect is of course loop suppressed [8, 9]. When we turn on the LFV terms, imaginary A_τ can induce a contribution to d_e at one loop level which can exceed the present bound on d_e by several orders of magnitude. The effect is demonstrated in Fig. 1. For illustrative purposes, in this figure, the off-diagonal elements of m_L^2 and m_R^2 are inserted on the relevant lines as a small perturbation. However, to make the analysis, we use the exact formula for d_e and do not use mass insertion approximation. The formulation can be found in the appendix of [8].

The strong bound on $\text{Br}(\mu \rightarrow e\gamma)$ [10] implies strong bounds on the $e\mu$ elements of m_L^2 , m_R^2 and A_{ij} . Throughout this paper we set the $e\mu$ elements of these matrices equal to zero. There are also strong bounds on $\text{Br}(\tau \rightarrow e\gamma)$ and

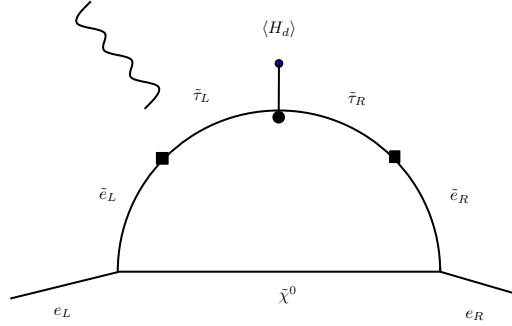


Figure 1: A neutralino exchange diagram contributing to d_e . The photon can attach to any of the \tilde{e}_L , $\tilde{\tau}_L$, $\tilde{\tau}_R$ or \tilde{e}_R propagators. The boxes on the left and right sides respectively depict insertion of $(m_L^2)_{e\tau}$ and $(m_R^2)_{\tau e}$. The circles indicate insertion of the A_τ vertex and the vacuum expectation value of H_d .

$\text{Br}(\tau \rightarrow \mu\gamma)$ [11] but these bounds are about three orders of magnitude less stringent than the bound on $\text{Br}(\mu \rightarrow e\gamma)$. Each of the LFV $e\tau$ and $\mu\tau$ elements can be sizeable (of order of the diagonal elements) without violating the present bounds. However if the τe and $\tau\mu$ elements are simultaneously present, both μ and e flavor will be violated and $\text{Br}(\mu \rightarrow e\gamma)$ can receive a contribution exceeding the present bound on it. To avoid such a situation, we set all the $\mu\tau$ elements equal to zero so the only sources of LFV in the present analysis are the $e\tau$ elements.

3. NEW CONTRIBUTIONS TO d_e IN THE PRESENCE OF LFV

In this section, we explore the effects of A_τ on d_e by presenting figures. To draw the figures, the mass spectrum corresponding to the α benchmark proposed in [12] has been chosen. However, the mass spectrum of the staus has been allowed to slightly deviate from that at the α benchmark. Notice that at this benchmark, the lightest stau is considerably heavier than the lightest neutralino so stau-neutralino coannihilation cannot play any significant role in fixing the dark matter relic density. As a result, a slight change of stau parameters will not dramatically affect the cosmological predictions. We have checked for robustness of the results and have found that the α benchmark is a typical point in the parameter space that demonstrate the overall behavior for most of the parameter space. More figures can be found in [8].

Fig. 2 shows d_e versus the sine of ϕ_{A_τ} for $A_{ij} = 0$ and various values of $(m_L^2)_{e\tau}$ and $(m_R^2)_{e\tau}$. To draw the dotted line marked with (a), $(m_L^2)_{e\tau}$ and $(m_R^2)_{e\tau}$ are both taken to be large. As seen from the figure, in this case the present bound on d_e (depicted by the horizontal line) puts a strong bound on the phase of A_τ . However, in the case that either $(m_L^2)_{e\tau}$ or $(m_R^2)_{e\tau}$ is very small (as in the case of dashed line (b) and solid line (c)), the bound is considerably relaxed. Figure 1 demonstrates the reason: In order for $\text{Im}[A_\tau]$ to contribute to d_e , both $(m_L^2)_{e\tau}$ and $(m_R^2)_{e\tau}$ have to be sizeable. Suppose in the future, rare decay $\tau \rightarrow e\gamma$ is detected which means “some” of the $e\tau$ elements are nonzero. By measuring only $\text{Br}(\tau \rightarrow e\gamma)$, one cannot determine the ratio $(m_L^2)_{e\tau}/(m_R^2)_{e\tau}$. However, if the number of the detected events is statistically significant, it will be possible to derive more information by studying the angular distribution of the final particles in the $\tau \rightarrow e\gamma$ decay [13].

Following [8], let us define

$$A_P = 4 \times \frac{\int_0^1 \frac{d\Gamma(\tau \rightarrow e\gamma)}{d\cos\theta} d\cos\theta - \int_{-1}^0 \frac{d\Gamma(\tau \rightarrow e\gamma)}{d\cos\theta} d\cos\theta}{\Gamma(\tau \rightarrow e\gamma)}. \quad (7)$$

where θ is the angle that the momentum of e makes with the spin of τ . In principle, A_P can be measured by studying the angular distribution of the final particles at an e^-e^+ collider such as a B-factory [13]. A_P is a measure of the

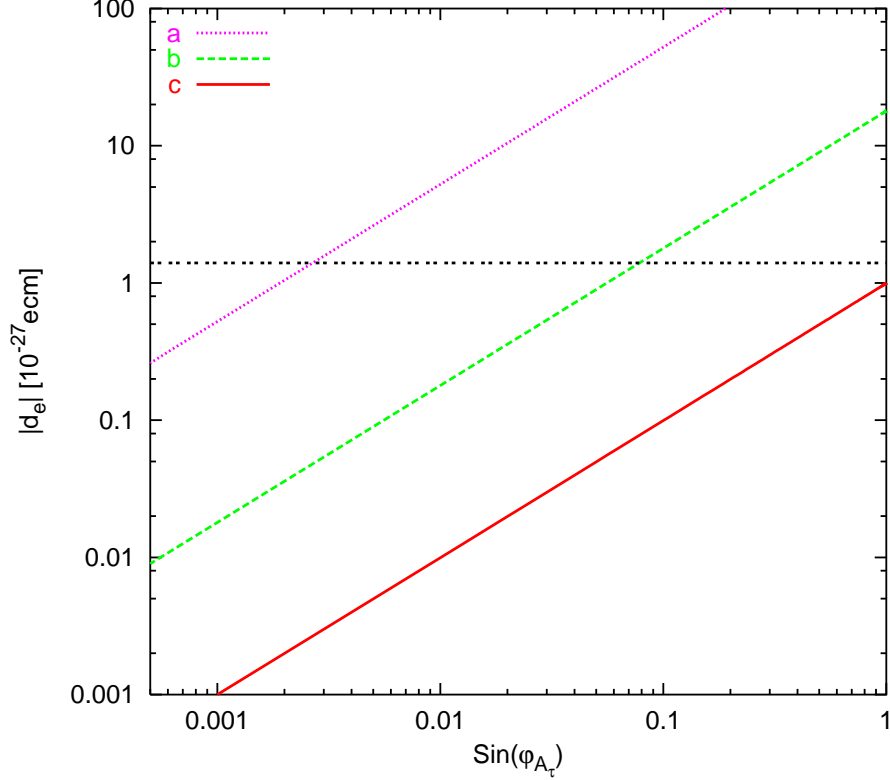


Figure 2: d_e versus $\sin\phi_{A_\tau}$. The input parameters correspond to the α benchmark proposed in [12]: $|\mu| = 375$ GeV, $m_0 = 210$ GeV, $M_{1/2} = 285$ GeV and $\tan\beta = 10$. We have set $|A_\tau|=500$ GeV. All the LFV elements of the slepton mass matrix are set to zero except $(m_L^2)_{e\tau}$ and $(m_R^2)_{e\tau}$. The dotted (pink) line labeled (a) corresponds to $(m_L^2)_{e\tau}=3500$ GeV² and $(m_R^2)_{e\tau}=15000$ GeV². The dashed (green) line labeled (b) corresponds to $(m_L^2)_{e\tau}=50$ GeV² and $(m_R^2)_{e\tau}=37000$ GeV². The solid (red) line labeled (c) corresponds to $(m_L^2)_{e\tau}=3500$ GeV² and $(m_R^2)_{e\tau}=30$ GeV². The horizontal dotted line at 1.4×10^{-27} e cm depicts the present experimental limit [10] on d_e .

hierarchy between left and right LFV elements. That is if $(m_R^2)_{e\tau} \ll (m_L^2)_{e\tau}$ and $A_{e\tau} \ll A_{\tau e}$, A_P converges to -1 . In the opposite case that $(m_R^2)_{e\tau} \gg (m_L^2)_{e\tau}$ and $A_{e\tau} \gg A_{\tau e}$, A_P converges to 1. Figs. (3-7) examine the correlation between A_P and d_e . To draw these plots we have assigned random values to the $e\tau$ elements of the slepton mass matrix in the range satisfying the present bound on $\text{Br}(\tau \rightarrow e\gamma)$ [11]. In Figs (3-5), we have set $|A_\tau| = 500$ GeV and assumed maximal value for the CP-violating phase: $\phi_{A_\tau} = \pi/2$. For the LF conserving parameters, we have taken the spectrum of the α benchmark [12]. Each pair of the scatter plots shown in Figs. (3-5) corresponds to different configurations of the $e\tau$ elements. To draw each pair, we have assigned random values (from a logarithmic scale) to various $e\tau$ elements. We have then calculated the corresponding values of $\text{Br}(\tau \rightarrow e\gamma)$, $|d_e|$ and A_P and have depicted the corresponding scatter points with the same color and symbol in figures (a) and (b). The horizontal lines at 1.4×10^{-27} e cm and 10^{-29} e cm respectively show the present bound [10] and the reach of the forthcoming experiments [2]. As seen from the figures, for a given value of $\text{Br}(\tau \rightarrow e\gamma)$, d_e cannot exceed a certain value.

In the case of Fig. 3, $A_{e\tau}$ and $A_{\tau e}$ are set equal to zero. As seen from the figure, for a significant portion of the parameter space, d_e lies above the present bound (the points shown with green (light grey) dots). The scatter points depicted by pink circle, which appear in Fig. 3-b as two pink horizontal lines at $A_P = \pm 1$, correspond to $d_e < 10^{-29}$ e cm. From Fig. 3-b we conclude that for $A_{e\tau} = A_{\tau e} = 0$, the bound on d_e can be satisfied if either $\text{Br}(\tau \rightarrow e\gamma)$ is very small (which means that all the LFV masses are very small) or A_P is close to ± 1 (meaning that there is a hierarchy between the LFV elements). In other words within this scenario, if future searches find

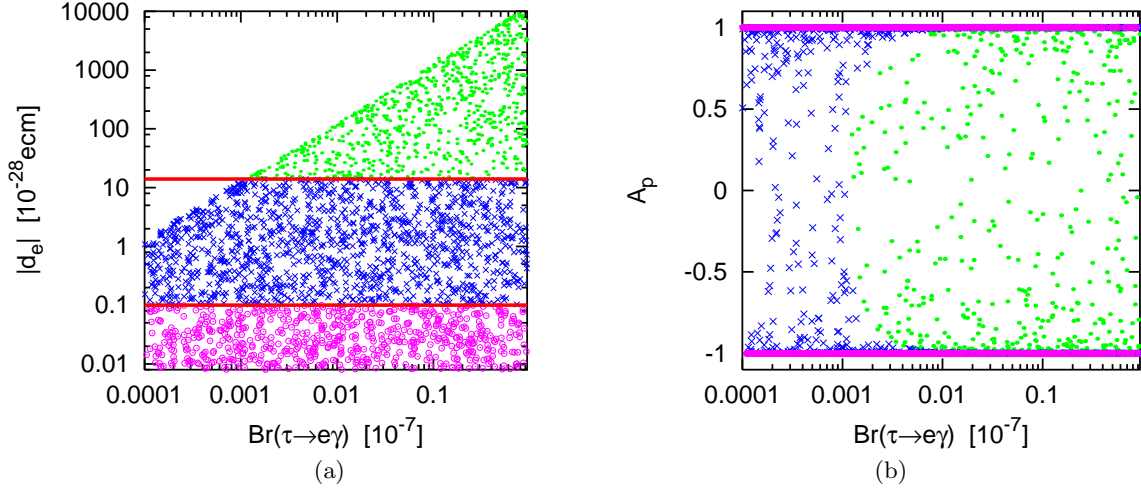


Figure 3: a) Scatter plot of d_e versus $\text{Br}(\tau \rightarrow e\gamma)$. The input parameters correspond to the α benchmark proposed in [12]: $|\mu| = 375$ GeV, $m_0 = 210$ GeV, $M_{1/2} = 285$ GeV and $\tan\beta = 10$. We have however set $\phi_{A_\tau} = \pi/2$ and $|A_\tau| = 500$ GeV. All the LFV elements of the slepton mass matrix are set to zero except $(m_{LR}^2)_{e\tau}$ and $(m_{LR}^2)_{\tau e}$ which pick up random values at a logarithmic scale respectively from $(5.9 \times 10^{-4} \text{ GeV}^2, 5.9 \times 10^3 \text{ GeV}^2)$ and $(3.7 \times 10^{-3} \text{ GeV}^2, 3.7 \times 10^4 \text{ GeV}^2)$. The horizontal line at $1.4 \times 10^{-27} e \text{ cm}$ depicts the present experimental limit [10] and the one at $10^{-29} e \text{ cm}$ shows the limit that can be probed in the near future [2]. b) Scatter plot of A_P versus $\text{Br}(\tau \rightarrow e\gamma)$. For each scatter point in Fig. 3-a there is a counterpart in Fig. 3-b corresponding to the same input values for the $e\tau$ elements which is shown with the same color and symbol. Notice that points shown in pink (corresponding to $d_e < 10^{-29} e \text{ cm}$) all lie on the horizontal lines at $A_p = \pm 1$.

$5 \times 10^{-10} < \text{Br}(\tau \rightarrow e\gamma)$ and $-0.9 < A_P < 0.9$, the bound on d_e should be interpreted either as a bound on ϕ_{A_τ} or as an indication for a cancelation between different contributions from ϕ_{A_τ} and other possible CP-violating phases.

To draw Fig. 4, $(m_{LR}^2)_{e\tau}$ and $(m_{LR}^2)_{\tau e}$ are set equal to zero and instead random values within a range are assigned to $(m_{LR}^2)_{e\tau}$ and $(m_{LR}^2)_{\tau e}$. The upper limit of the range (*i.e.*, 780 GeV^2) saturate the constraints from the Unbounded From Below (UFB) consideration [14]. Notice that these bounds on $(m_{LR}^2)_{e\tau}$ and $(m_{LR}^2)_{\tau e}$ imply a “theoretical” bound on $\text{Br}(\tau \rightarrow e\gamma)$. The scatter points at the tilted peak with highest d_e and $\text{Br}(\tau \rightarrow e\gamma)$ correspond to the cases that both $(m_{LR}^2)_{e\tau}$ and $(m_{LR}^2)_{\tau e}$ are close to the upper limit. Notice that a correlation between d_e , A_P and $\text{Br}(\tau \rightarrow e\gamma)$ similar to that in the case of Fig. 3 emerges. That is the points marked with green dots (corresponding to $d_e > 1.4 \times 10^{-27} e \text{ cm}$), with blue “ \times ” (corresponding to $10^{-29} < d_e < 1.4 \times 10^{-27} e \text{ cm}$) and with pink circles (corresponding to $d_e < 10^{-29} e \text{ cm}$) are respectively scattered from right to left. Notice however that in contrast to Fig. 3-b, Fig. 4-b includes scatter points with $-0.9 < A_P < 0.9$ and $\text{Br}(\tau \rightarrow e\gamma) \sim 10^{-8}$ that satisfy the present bound on d_e (the points marked with “ \times ” in the plot). In Fig. 6, we have repeated the same analysis with the δ benchmark [12]. In the case of the δ benchmark, the constraint from the UFB is so stringent that for all scatter points $d_e < 2 \times 10^{-28} e \text{ cm}$ and $\text{Br}(\tau \rightarrow e\gamma) < 2 \times 10^{-9}$.

In Fig. 5, $(m_{LR}^2)_{e\tau}$, $(m_{LR}^2)_{\tau e}$, $(m_{LR}^2)_{e\tau}$ and $(m_{LR}^2)_{\tau e}$ all take nonzero random values. Fig. 5-a contains features of both Figs. 3-a and 4-a. The significant point is that setting all the $e\tau$ mass elements nonzero, the correlation among A_P , d_e and $\text{Br}(\tau \rightarrow e\gamma)$ becomes weaker. That is, unlike Figs. 3-b and 4-b, Fig. 5-b contains points below the sensitivity limit of the forthcoming d_e searches (points depicted with pink circles with $d_e < 10^{-29} e \text{ cm}$) for which $\text{Br}(\tau \rightarrow e\gamma) > 10^{-8}$ and $-0.9 < A_P < 0.9$. This can be explained as follows. At scatter points for which

$$[(m_{LR}^2)_{e\tau}, (m_{LR}^2)_{e\tau} \ll (m_{LR}^2)_{\tau e}, (m_{LR}^2)_{\tau e}] \text{ or } [(m_{LR}^2)_{e\tau}, (m_{LR}^2)_{e\tau} \gg (m_{LR}^2)_{\tau e}, (m_{LR}^2)_{\tau e}], \quad (8)$$

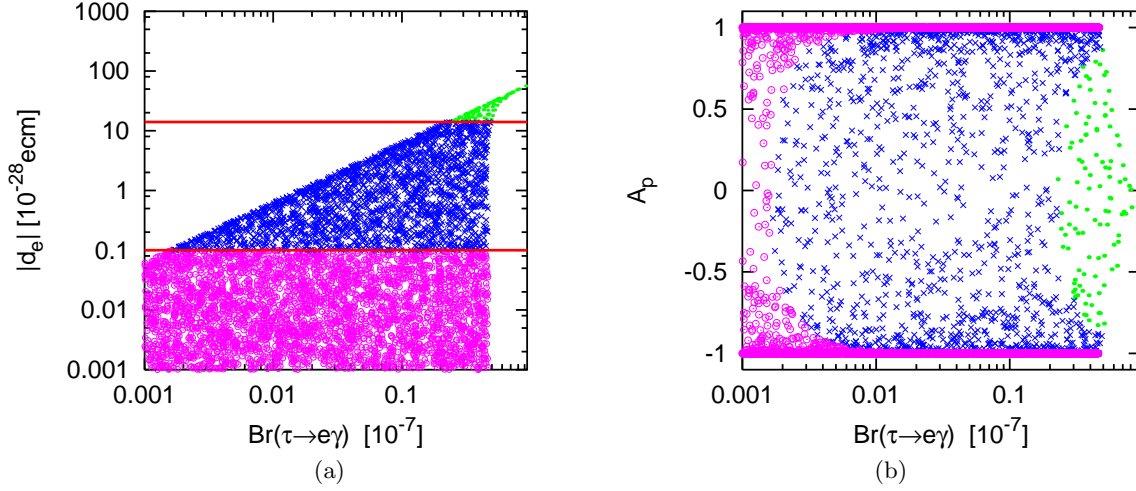


Figure 4: Similar to Fig. 3 except that $(m_L^2)_{e\tau} = (m_R^2)_{e\tau} = 0$ and instead $(m_{LR}^2)_{e\tau} (= A_{e\tau}\langle H_d \rangle)$ and $(m_{LR}^2)_{\tau e} (= A_{\tau e}\langle H_d \rangle)$ pick up random values at a logarithmic scale from $(7.8 \times 10^{-4} \text{ GeV}^2, 7.8 \times 10^2 \text{ GeV}^2)$. For each scatter point in Fig. 4-a there is a counterpart in Fig. 4-b corresponding to the same input values for the $e\tau$ elements which is shown with the same color and symbol.

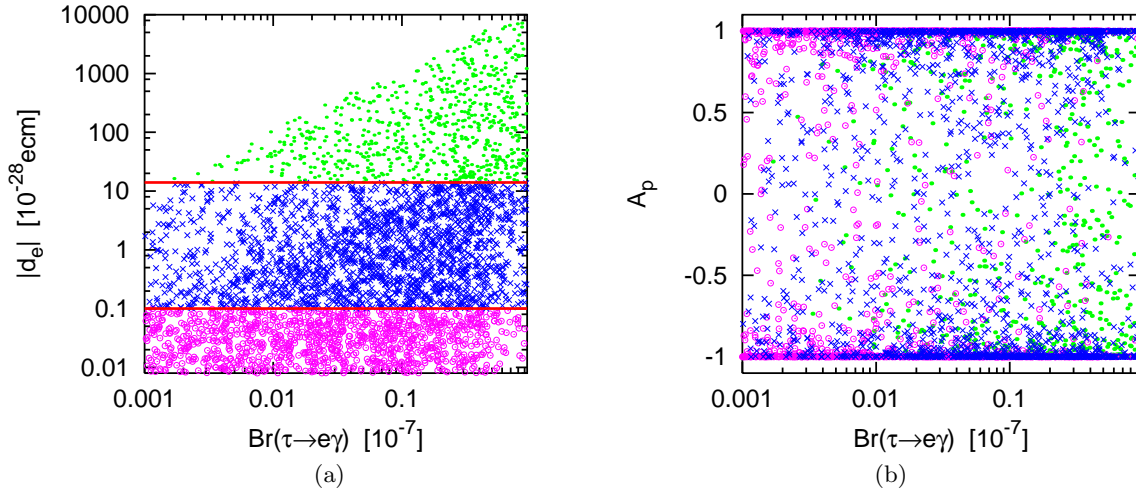


Figure 5: Similar to Fig. 3 except that here in addition to $(m_L^2)_{e\tau}$ and $(m_R^2)_{e\tau}$, $(m_{LR}^2)_{e\tau} (= A_{e\tau}\langle H_d \rangle)$ and $(m_{LR}^2)_{\tau e} (= A_{\tau e}\langle H_d \rangle)$ are also allowed to be nonzero. The values of $(m_L^2)_{e\tau}$ and $(m_R^2)_{e\tau}$ are randomly chosen respectively from $(5.9 \times 10^{-3} \text{ GeV}^2, 5.9 \times 10^3 \text{ GeV}^2)$ and $(3.7 \times 10^{-2} \text{ GeV}^2, 3.7 \times 10^4 \text{ GeV}^2)$ at a logarithmic scale. $(m_{LR}^2)_{e\tau}$ and $(m_{LR}^2)_{\tau e}$ pick up random values at a logarithmic scale from the interval $(0.78 \text{ GeV}^2, 780 \text{ GeV}^2)$. For each scatter point in Fig. 5-a there is a counterpart in Fig. 5-b corresponding to the same input values for the $e\tau$ elements which is shown with the same color and symbol.

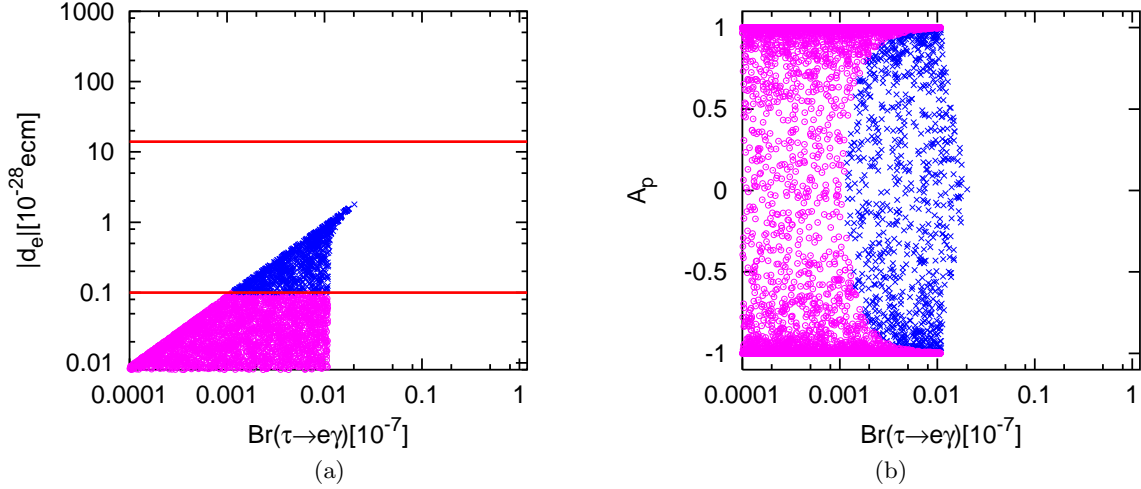


Figure 6: a) Scatter plot of d_e versus $\text{Br}(\tau \rightarrow e\gamma)$. The input parameters correspond to the δ benchmark proposed in [12]: $|\mu| = 930$ GeV, $m_0 = 500$ GeV, $M_{1/2} = 750$ GeV and $\tan\beta = 10$. We have however set $\phi_{A_\tau} = \pi/2$ and $|A_\tau| = 1800$ GeV. $(m_L^2)_{e\tau}$ and $(m_R^2)_{e\tau}$ are zero but $(m_{LR}^2)_{e\tau}$ and $(m_{LR}^2)_{\tau e}$ pick up random values from $(0.18 \text{ GeV}^2, 1.8 \times 10^3 \text{ GeV}^2)$. The horizontal line at $1.4 \times 10^{-27} e \text{ cm}$ depicts the present experimental limit [10] and the one at $10^{-29} e \text{ cm}$ shows the limit that can be probed in the near future [2]. b) Scatter plot of A_P versus $\text{Br}(\tau \rightarrow e\gamma)$. For each scatter point in Fig. a there is a counterpart in Fig. b corresponding to the same input values for the $e\tau$ elements which is shown with the same color and symbol. Notice that points shown in pink (corresponding to $d_e < 10^{-29} e \text{ cm}$) all lie on the horizontal lines at $A_P = \pm 1$.

A_L can be of order of A_R which yields $-0.9 < A_P < 0.9$ but despite sizeable ϕ_{A_τ} , d_e is still small. Pink circles lying in the region $\text{Br}(\tau \rightarrow e\gamma) > 10^{-9}$ and $-0.9 < A_P < 0.9$ correspond to such configurations. As a result, without independent knowledge of the ratios of LFV elements, we cannot derive any conclusive bound on ϕ_{A_τ} . The fraction of the scatter points with $d_e < 10^{-29} e \text{ cm}$ (pink circles) lying in the region with $-0.9 < A_P < 0.9$ and $10^{-8} < \text{Br}(\tau \rightarrow e\gamma)$ strongly depends on the choice of the range and scale of random pick up of the LFV input. For example, had we chosen the lower limit of the range of $(m_L^2)_{e\tau}$ and $(m_R^2)_{e\tau}$ two orders of magnitude higher [*i.e.*, $(m_L^2)_{e\tau} \in (0.59 \text{ GeV}^2, 5900 \text{ GeV}^2)$ and $(m_R^2)_{e\tau} \in (3.7 \text{ GeV}^2, 37000 \text{ GeV}^2)$ instead of $(m_L^2)_{e\tau} \in (0.0059 \text{ GeV}^2, 5900 \text{ GeV}^2)$ and $(m_R^2)_{e\tau} \in (0.037 \text{ GeV}^2, 37000 \text{ GeV}^2)$], no pink circles would have in practice appeared in this region. This is understandable because for a constant number of the scatter points, decreasing the lower limit of $(m_L^2)_{e\tau}$ and $(m_R^2)_{e\tau}$ increases the weight of the region for which condition in Eq. (8) is satisfied.

If by some theoretical consideration we exclude the possibility of conditions (8), the correlation between A_P and d_e is maintained so, for $\text{Br}(\tau \rightarrow e\gamma) \gtrsim 10^{-8}$ and $-0.9 < A_P < 0.9$, the present bound on d_e can be interpreted as a strong bound on ϕ_{A_τ} [8]. For example within the scenario described in [15] which relates all the LFV elements to the Yukawa couplings, conditions (8) cannot be fulfilled. Moreover, in some parts of the parameter space, by combining information from different observables with the UFB bounds on the LFV elements of m_{LR}^2 , we can exclude the possibility of Eq. (8). This is demonstrated in Figs. 6 and 7. As seen from Fig. 6, at the δ benchmark, the bounds from UFB exclude the possibility of a contribution from $(m_L^2)_{e\tau}$ and $(m_R^2)_{e\tau}$ to $\text{Br}(\tau \rightarrow e\gamma)$ at the level of $O(10^{-8})$. Thus, if the δ benchmark is established at LHC and $\text{Br}(\tau \rightarrow e\gamma)$ turns out to be of order of 10^{-8} , we will conclude that the contributions comes from $(m_L^2)_{e\tau}$ and/or $(m_R^2)_{e\tau}$. Moreover if observation shows that $-0.9 < A_P < 0.9$, we will conclude that the contributions of $(m_L^2)_{e\tau}$ and $(m_R^2)_{e\tau}$ are comparable so the conditions in Eq. (8) cannot be fulfilled. In fact, Fig. 7 shows that at the δ benchmark, the correlation between A_P and d_e is maintained even when all the $e\tau$ elements pick up nonzero values within the allowed region. Fig. 7 shows that for $\text{Br}(\tau \rightarrow e\gamma) > 10^{-8}$

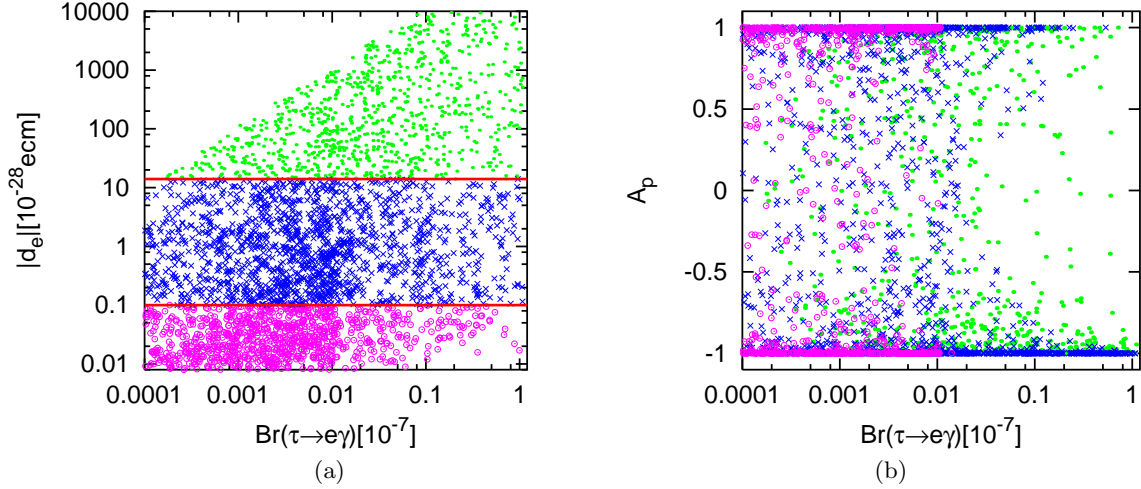


Figure 7: a) Scatter plot of d_e versus $\text{Br}(\tau \rightarrow e\gamma)$. The input parameters correspond to the δ benchmark proposed in [12]: $|\mu| = 930$ GeV, $m_0 = 500$ GeV, $M_{1/2} = 750$ GeV and $\tan\beta = 10$. We have however set $\phi_{A_\tau} = \pi/2$ and $|A_\tau| = 1800$ GeV. $(m_{L}^2)_{e\tau}$ and $(m_{R}^2)_{e\tau}$ respectively pick up random values at a logarithmic scale respectively from $(0.23 \text{ GeV}^2, 2.3 \times 10^5 \text{ GeV}^2)$ and $(0.33 \text{ GeV}^2, 3.3 \times 10^5 \text{ GeV}^2)$. $(m_{LR}^2)_{e\tau}$ and $(m_{LR}^2)_{\tau e}$ pick up random values from $(0.18 \text{ GeV}^2, 1.8 \times 10^3 \text{ GeV}^2)$. The horizontal line at $1.4 \times 10^{-27} e \text{ cm}$ depicts the present experimental limit [10] and the one at $10^{-29} e \text{ cm}$ shows the limit that can be probed in the near future [2]. b) Scatter plot of A_p versus $\text{Br}(\tau \rightarrow e\gamma)$. For each scatter point in Fig. a there is a counterpart in Fig. b corresponding to the same input values for the $e\tau$ elements which is shown with the same color and symbol. Notice that points shown in pink (corresponding to $d_e < 10^{-29} e \text{ cm}$) all lie on the horizontal lines at $A_p = \pm 1$.

and $-0.5 < A_p < 0.5$, $\phi_{A_\tau} = \pi/2$ yields d_e higher than the present bound: $d_e > 1.4 \times 10^{-27} e \text{ cm}$. Moreover for $\text{Br}(\tau \rightarrow e\gamma) > 10^{-9}$ and $-0.9 < A_p < 0.9$, $\phi_{A_\tau} = \pi/2$ yields d_e detectable in forthcoming experiments: $d_e > 10^{-29} e \text{ cm}$.

4. CONCLUSIONS AND OUTLOOK

We have shown that in the presence of the $e\tau$ LFV elements, the phase of A_τ , ϕ_{A_τ} , can contribute to d_e at one loop level. For values of $\text{Br}(\tau \rightarrow e\gamma)$ close to the present experimental bounds, the contribution of ϕ_{A_τ} to d_e can exceed the experimental bound on d_e by several orders of magnitude. We have found that even if $\text{Br}(\tau \rightarrow e\gamma)$ is three orders of magnitude below the present bound, the contribution to d_e can still exceed the present bound on d_e . The effect of ϕ_{A_τ} on d_e strongly depends on the ratios of the LFV slepton masses $(m_{L}^2)_{e\tau}/(m_{R}^2)_{e\tau}$ and $(m_{LR}^2)_{e\tau}/(m_{LR}^2)_{\tau e}$. In other words, for a given value of $\text{Br}(\tau \rightarrow e\gamma)$ and ϕ_{A_τ} , $|d_e|$ can take any value between zero and a maximum which depends on the value of $\text{Br}(\tau \rightarrow e\gamma)$ and ϕ_{A_τ} [see Figs. (3-a)-(7-a)]. We have shown that for the specific case that $(m_{LR}^2)_{e\tau} = (m_{LR}^2)_{\tau e} = 0$ (see Fig. 3-b) or $(m_{L}^2)_{e\tau} = (m_{R}^2)_{e\tau} = 0$ [see Fig. 4-b], by measuring the asymmetry A_p defined in Eq. (7) we can solve this ambiguity. However, in the general case that all the $e\tau$ elements are nonzero, as shown in Fig. 5, the correlation between A_p and d_e becomes weaker and to solve the ambiguity, extra information is needed.

Let us suppose that $\text{Br}(\tau \rightarrow e\gamma)$ turns out to be close to the present bound (*i.e.*, $\text{Br}(\tau \rightarrow e\gamma) > 10^{-8}$) and moreover let us suppose A_p is measured and found to be $-0.9 < A_p < 0.9$. Excluding the possibility of a fine tuned cancellation between the contributions of different phases, two possibilities emerge: 1) ϕ_{A_τ} is smaller than $O(0.005)$; 2) ϕ_{A_τ} is large but one of the conditions in Eq. (8) is fulfilled. To derive a conclusive bound on ϕ_{A_τ} , the second possibility has

to be excluded. We show that at some parts of the parameter space such as the δ benchmark, the second possibility is excluded by bounds on $(m_{LR}^2)_{e\tau}$ and $(m_{LR}^2)_{\tau e}$ from the UFB consideration.

In summary, combining the information on d_e and LFV τ decay modes gives invaluable information on $\phi_{A\tau}$. In certain parts of the parameter space (*e.g.*, the δ benchmark), by studying these observables, we can constrain $\phi_{A\tau}$ however in other parts (*e.g.*, the α benchmark) drawing conclusive bounds on $\phi_{A\tau}$ is not possible. In the latter case, this method cannot replace the direct measurement of $\phi_{A\tau}$ at ILC. On the other hand, direct measurement of $\phi_{A\tau}$ at ILC can help us to resolve the degeneracies in the pattern of the LFV elements.

Acknowledgments

Y.F. would like to thank the organizers of ICHEP 08 for giving her the opportunity to present this talk.

References

- [1] F. Hoogeveen, Nucl. Phys. B **341** (1990) 322. M. E. Pospelov and I. B. Khriplovich, Sov. J. Nucl. Phys. **53** (1991) 638 [Yad. Fiz. **53** (1991) 1030]; M. J. Booth, arXiv:hep-ph/9301293.
- [2] D. Kawall, F. Bay, S. Bickman, Y. Jiang and D. DeMille, AIP Conf. Proc. **698** (2004) 192; D. Kawall, F. Bay, S. Bickman, Y. Jiang and D. DeMille, Phys. Rev. Lett. **92** (2004) 133007 [arXiv:hep-ex/0309079]; S. K. Lamoreaux, Phys. Rev. D **66** (2002) 010001 arXiv:nucl-ex/0109014.
- [3] A. de Gouvea and S. Gopalakrishna, Phys. Rev. D **72**, 093008 (2005) [arXiv:hep-ph/0508148].
- [4] S. T. Petcov, Sov. J. Nucl. Phys. **25**, 340 (1977) [Yad. Fiz. **25**, 641 (1977) ERRAT,25,698.1977 ERRAT,25,1336.1977]; S. M. Bilenky, S. T. Petcov and B. Pontecorvo, Phys. Lett. B **67**, 309 (1977); G. Altarelli, L. Baulieu, N. Cabibbo, L. Maiani and R. Petronzio, Nucl. Phys. B **125**, 285 (1977) [Erratum-ibid. B **130**, 516 (1977)].
- [5] K. A. Olive, M. Pospelov, A. Ritz and Y. Santoso, Phys. Rev. D **72** (2005) 075001 [arXiv:hep-ph/0506106]; S. Abel, S. Khalil and O. Lebedev, Nucl. Phys. B **606** (2001) 151 [arXiv:hep-ph/0103320]; T. Falk *et al.*, Nucl. Phys. B **560** (1999) 3 [arXiv:hep-ph/9904393]; A. Afanasev, C. E. Carlson and C. Wahlquist, Phys. Rev. D **61** (2000) 034014 [arXiv:hep-ph/9903493]; T. Ibrahim and P. Nath, Phys. Lett. B **418** (1998) 98 [arXiv:hep-ph/9707409]; M. Brhlik, G. J. Good and G. L. Kane, Phys. Rev. D **59** (1999) 115004 [arXiv:hep-ph/9810457]; A. Bartl *et al.*, Phys. Rev. D **60** (1999) 073003 [arXiv:hep-ph/9903402]; T. Falk, K. A. Olive, M. Pospelov and R. Roiban, Nucl. Phys. B **560** (1999) 3 [arXiv:hep-ph/9904393]; S. Yaser Ayazi and Y. Farzan, Phys. Rev. D **74**, 055008 (2006) [arXiv:hep-ph/0605272]; S. Y. Ayazi, *In the Proceedings of IPM School and Conference on Lepton and Hadron Physics (IPM-LHP06), Tehran, Iran, 15-20 May 2006, pp 0004* [arXiv:hep-ph/0611056].
- [6] P. Nath, Phys. Rev. Lett. **66** (1991) 2565 ; Y. Kizukuri and N. Oshimo, Phys. Rev. D **46** (1992) 3025; V. A. Kuzmin, V. A. Rubakov and M. E. Shaposhnikov, Phys. Lett. B **155**, 36 (1985); V. Cirigliano, S. Profumo and M. J. Ramsey-Musolf, JHEP **0607**, 002 (2006) [arXiv:hep-ph/0603246] K. A. Olive, M. Pospelov, A. Ritz and Y. Santoso, Phys. Rev. D **72** (2005) 075001 [arXiv:hep-ph/0506106]; T. Falk and K. A. Olive, Phys. Lett. B **375** (1996) 196 [arXiv:hep-ph/9602299]; T. Ibrahim and P. Nath, arXiv:hep-ph/0210251.
- [7] A. Bartl, W. Majerotto, W. Porod and D. Wyler, Phys. Rev. D **68** (2003) 053005 [arXiv:hep-ph/0306050]; W. Porod, *Prepared for International Workshop on Astroparticle and High-Energy Physics (AHEP-2003), Valencia, Spain, 14-18 Oct 2003*.
- [8] S. Y. Ayazi and Y. Farzan, JHEP **0706**, 013 (2007) [arXiv:hep-ph/0702149].
- [9] D. Chang, W. Y. Keung and A. Pilaftsis, Phys. Rev. Lett. **82** (1999) 900 [Erratum-ibid. **83** (1999) 3972] [arXiv:hep-ph/9811202].
- [10] W.-M. Yao *et al.*, J. Phys. G **33** (2006) 1.
- [11] S. Banerjee, Nucl. Phys. Proc. Suppl. **169** (2007) 199 [arXiv:hep-ex/0702017].

- [12] A. De Roeck, J. R. Ellis, F. Gianotti, F. Moortgat, K. A. Olive and L. Pape, *Eur. Phys. J. C* **49**, 1041 (2007) [arXiv:hep-ph/0508198].
- [13] R. Kitano and Y. Okada, *Phys. Rev. D* **63** (2001) 113003 [arXiv:hep-ph/0012040].
- [14] J. A. Casas and S. Dimopoulos, *Phys. Lett. B* **387**, 107 (1996) [arXiv:hep-ph/9606237].
- [15] L. Calibbi, J. Jones-Perez and O. Vives, arXiv:0804.4620 [hep-ph].